Systematic coformer contribution to cocrystal stabilization : energy and packing trends

Systematic coformer contribution to cocrystal stabilization: energy and packing trends

Paolo P. Mazzeo,[a,b] Stefano Canossa,[a‡] Claudia Carraro,[a] Paolo Pelagatti[a,c] and Alessia Bacchi*[a,b]

[a] Dipartimento di Scienze Chimiche, della Vita e della Sostenibilità Ambientale, Università degli Studi di Parma, Via Parco Area delle Scienze 17/A, 43124 Parma, Italy

[b] Biopharmanet-TEC, Università degli Studi di Parma, via Parco Area delle Scienze 27/A, 43124 Parma, Italy. E-mail: alessia.bacchi@unipr.it

[c] Consorzio Interuniversitario di Reattività Chimica e Catalisi (CIRCC), Via Celso Ulpiani 27, 70126 Bari, Italy

[‡] Current affiliation: EMAT, Department of Physics, University of Antwerp, Groenenborgerlaan 171, 2020 Antwerp, Belgium.

Abstract. Polycyclic aromatic compounds such as acridine and phenazine are popular molecular partners used in cocrystal synthesis. The intermolecular interactions occurring between coformer and the molecular partner dominate the cocrystal packing energy, but coformer self-interactions might participate with a constance non-negligible contribution to the overall packing energy stabilization. Two new acridine-based cocrystals have been mechanochemically synthesized, then fully characterized *via* DSC and SCXRD analyses. A statistical analysis in the CSD has been performed to evaluate the recurrent π-π stacking orientation of the polycyclic coformer in all deposited acridine-based cocrystals, then extended to phanazine-base analogs. Packing Energy Calculation were performed on a selected cocrystals subset to quantify the contribution of the π-π interaction to the overall stabilization energy.

Introduction

In a long-lasting partnership, it is important not only that the two partners get well together, but also that each of them brings their own values in the couple.

Cocrystals are multicomponent crystalline materials made by different neutral chemical entities in a stoichiometric ratio[1–3]: designing a cocrystal requires a thorough knowledge of the possible supramolecular affinity between the molecular partners[4–10], which is at the basis of crystal engineering[6,11–14]. Appropriate interactions between the molecular partner and suitable coformers should provide a robust intermolecular network, thus significantly affecting the final properties of the material[15–23]. Recently, we explored the stabilization of liquid components by cocrystallisation combining them with suitable molecular coformers[17,21,24]. The strategy behind the selection of the best coformers is typically limited by the ability of the two partners to directly establish strong supramolecular synthons[25–28] based on hydrogen bonds[29–31]or other intermolecular contacts[32,33], hence, if the molecule of interest brings an intermolecular bond donor group, the ideal coformer has to be decorated with an appropriate acceptor functional group[34]. However, coformer-coformer interactions are generally neglected in the classification of ideal coformers candidate.[10] Polycyclic aromatic compounds such as acridine or phenazine (scheme 1), are quite largely used as coformers[35–40] due to the absence of torsional degrees of freedom and their easily accessible H-bond acceptor groups. However, the molecular flatness of this two coformers is anyhow a predominant characteristic which heavily influence their mutual orientation within a crystal lattice and, by consequence, contributes to the overall stabilization of the final cocrystal structure[41,42]. In this paper we want to systematically investigate the contribution of self-interactions of these coformers to the packing energy in cocrystals obtained with a series of phenol derivates (hereinafter generically referred as molecule of interest ≡ MI) (scheme 1). This approach was already proposed in the literature by Hunter[34,43–47], Lo Presti[48–50] and others[41,51–54] referred to virtual cocrystal screening or cocrystal prediction; we here want to emphasize that these coformers typically participate with a constant contribution to the overall cocrystal packing energy due to a recurrent self-interaction path. To validate this approach, a statistical analysis[49] using the CCDC Cambridge Structural Database (CSD)[55] has been performed over all deposited cocrystals containing acridine or phenazine.

Scheme 1. Molecules involved in the study.

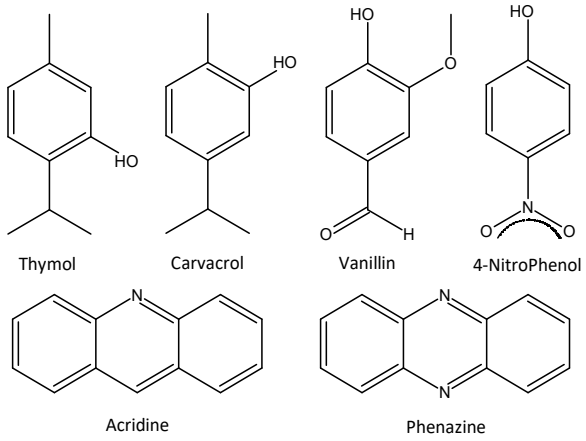

Results and discussion

Exploring the concept of using coformers able to contribute with homo-interactions to the overall cocrystal stabilization, we here report two newly synthesized cocrystals, namely Acr:Thy (Acridine:Thymol 1:1) and Acr:Car (Acridine:Carvacrol 1:2). In both cocrystals acridine is the coformer, while thymol and carvacrol, two isomeric components of natural essential oils extracted from thyme[56] and oregano[57], are the ingredient of interest (scheme 1). Crystal structures of the newly discovered cocrystals were solved *via* SCXRD analyses; crystal data are reported in table 1 (for the extended version see ESI).

In Acr:Thy, acridine and thymol cocrystallize in the $P2_1/c$ space-group in a 1:1 stoichiometry ratio with one formula unit and two independent molecules in the asymmetric unit (Z'=1, Z''=2)[58]. Two pairs of hydrogen bonded acridine and thymol molecules (donor-acceptor distance of N-O = 2.796(3) Å) are assembled in dimers built by the stacking of two polycyclic molecules generated by an inversion centre (interplanar distance of 3.672(4) Å) (Fig. 1a). Each acridine molecule of the dimer alternately interacts with the thymol partner of the adjacent arrays as reported in figure 1b. Dimers are arranged in antiparallel arrays along the *c*-axis (fig. 2c) with no direct interaction between acridine pairs (fig. 2a, 2b).

In Acr:Car, acridine and carvacrol cocrystallize in the $P2_1/c$ space-group in a 1:2 stoichiometry ratio with one formula unit and three independent molecules in the asymmetric unit (Z'=1, Z''=3)[58]. Two pairs of hydrogen bonded acridine and carvacrol molecules (donor-acceptor distance of N-O = 2.711(5) Å) are assembled in dimers built by the stacking of two polycyclic molecules generated by an inversion centre (interplanar distance of 3.331(4) Å, Fig.3a). The carvacrol molecule directly bonded to the acridine coformer is bridging a second carvacrol molecule through another H-bond established from their hydroxyl groups (O-O donor-acceptor distance 2.861(2) Å). Each acridine molecule within the dimer alternately interacts with the carvacrol molecules of different adjacent arrays as reported in figure 3b.

$Acr:Car_2$ dimers are piled along the crystallographic *a*-direction even though largely offset (offset 5.362(1) Å, interplanar distance 3.545(4) Å, centroid(B)-centroid(C) distance 8.428(4) Å) as shown in figures 4a and 4b.

Table 1. Crystal data and structure refinement for Acr:Thy 1:1 and Acr:Car 1:2

	Acr:Thy	**Acr:Car**
Empirical formula	$C_{23}H_{23}NO$	$C_{33}H_{37}NO_2$
Formula weight	329.45	479.63
Crystal system	monoclinic	monoclinic
Space group	$P2_1/c$	$P2_1/c$
a/Å	12.1372(1)	9.5596(4)
b/Å	9.1209(1)	34.544(1)
c/Å	17.2439(2)	9.0322(3)
α/°	90	90
β/°	108.629(1)	113.902(5)
γ/°	90	90
Volume/Å^3	1808.92(3)	2726.9(2)
Z	4	4
Final R indexes [I>=2σ (I)]	R_1 = 0.0617, wR_2 = 0.1611	R_1 = 0.0570, wR_2 = 0.1202
Largest ΔF max/min /e Å^{-3}	0.46/-0.51	0.23/-0.19

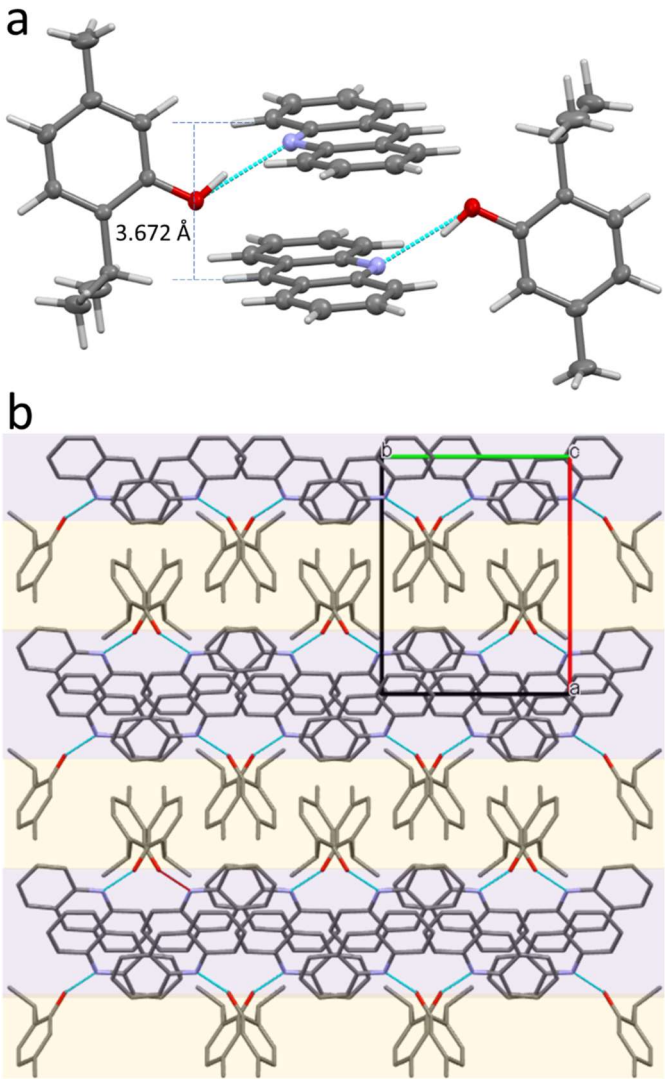

Figure 1. Acr:Thy 1:1. a) Detail of the interactions between molecular partners within the crystal structure; non-H atoms are reported in ellipsoid style while H atoms are reported in stick style. b) Crystal packing along the *b*-axis, hydrogen atoms are omitted for the sake of clarity; acridine and thymol columns are highlighted in purple and yellow respectively. Atoms are coloured according to the colour code C=grey, N=blue, O=red. H-bonds are reported as dotted cyan lines.

Faced acridine dimers are arranged in antiparallel arrays along the *b*-axis (fig 4c). In both cocrystals, in addition to the hydrogen bond interactions, acridine-acridine dispersive π-π interactions within dimers contribute to the overall cocrystal stabilization (fig. 1a and 3a): in Acr:Thy and Acr:Car, the two faced acridines are parallel oriented, respectively offset by 0.897(5) Å and 1.456(6) Å with a centroid-centroid distance of 3.780(3) Å and 3.653(2) Å, respectively.

Offset between two paired acridine molecules is calculated as the distance between the centroid of the first molecule and the projection of the centroid of the second molecules onto the molecular plane of the first molecule as reported in figure SI7.

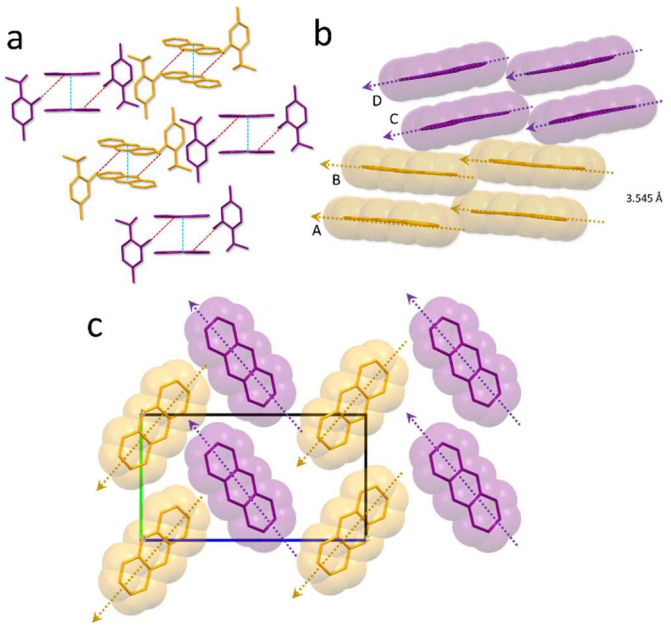

Figure 2. Acr:Thy 1:1 a) Representation of Acr:Thy interactions between dimers and molecular neighbours. Red dotted lines represent Acr···Thy H-bond interactions, cyan dotted lines represent Acr···Acr π-π interactions. b) Acridine parallel arrangement within dimers (A-B, C-D) and non-parallel arrangement between dimers (B-C). c) Acridine antiparallel arrangement along the c-axis. H-atoms are omitted for the sake of clarity.

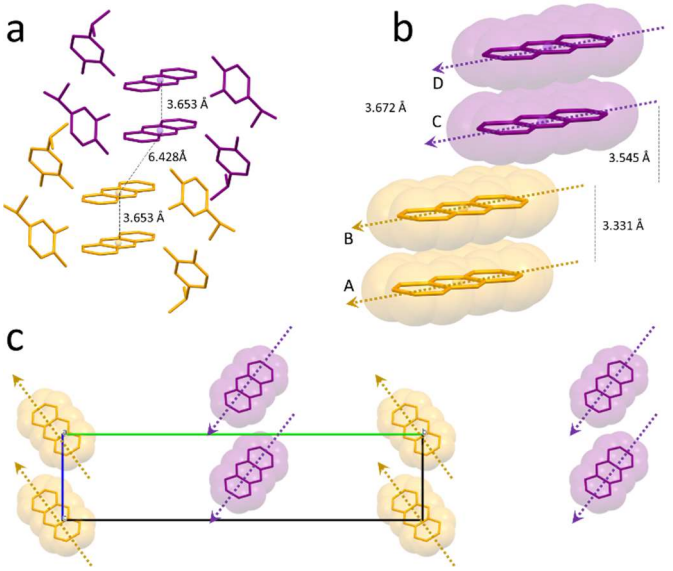

Figure 4. Acr:Car 1:2 a) Representation of Acr:Car_2 dimers arrangement; short and long centroid-centroid distances between acridine molecules respectively within and between dimers are reported. b) Acridine parallel arrangement within dimers (A-B and C-D) and between dimers (B-C) with relative interplanar distances. c) Acridine antiparallel arrangement along the *b*-axis.

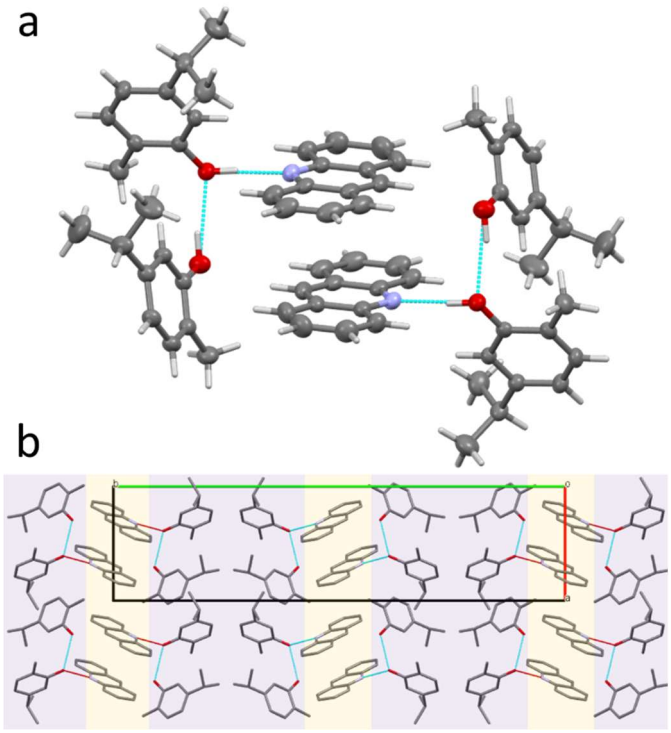

Figure 3. Acr:Car 1:2. a) Detail of intermolecular interactions in Acr:Car_2 dimer; non-H atoms are reported in ellipsoid style while H atoms are reported in stick style. b) crystal packing along the *c*-axis; H-atoms are omitted for the sake of clarity; acridine and carvacrol columns are highlighted in yellow and purple respectively. Atoms are coloured according to the colour code C=grey, N=blue, O=red. H-bonds are reported as dotted cyan lines.

At this point, we have investigated the relevance of the contribution of these homomeric coformer-coformer interactions to the overall stabilization of the cocrystal.

Energy frameworks[59] may help to understand the main contribution of the packing energy. This method visualises the interactions between molecular pairs, partitioning the interaction energy into coulombic and dispersive contribution. Energy frameworks calculated with CrystalExplorer[60] for Acr:Thy and Acr:Car at the B3LYP/6-31G(d,p) level of theory are reported in figures 5 and 6 and show that the packing stabilization arises mainly from a Coulombic contribution related to the Thy···Acr (fig. 5a) and Car···Acr (fig. 6a) hydrogen bonds, and a dispersive term related to the Acr···Acr stacking (fig. 5b, 6b). From the energy point of view, this is translated in a stabilising energy contribution of respectively -46.1 – -55.1 kJ mol^{-1} (coulombic) and -31.5 – -41.5 kJ mol^{-1} (dispersive), as resulted from the energy framework calculations. For a more detailed picture of the numerical values of the energy between molecular pairs, the reader should refer to figures SI8 and SI9. The acridine-acridine orientation and the attached dispersive energy contribution to the overall lattice energy stabilization are quite similar in both the cocrystals just described. In fact, similar orientation and π-π contribution have been observed in their phenazine-based cocrystals analogs recently reported in the literature.[17]

As polycyclic aromatic molecules, phenazine and acridine typically interact via π-π or CH-π contacts within the crystal lattice, therefore, CCDC Crystal Structure database has been used to analyse the phenazine-phenazine (P-P) and acridine-acridine (A-A) reciprocal orientation either in their pure phases

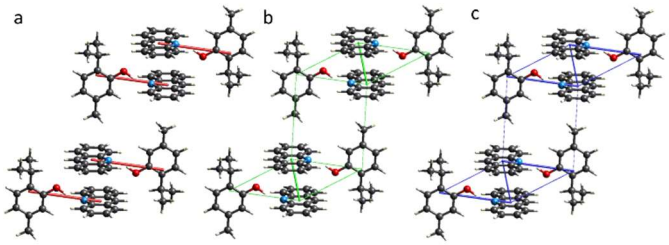

Figure 5. Energy framework calculation performed on Acr:Thy 1:1 at the B3LYP/6-31G(d,p) level of theory: a) Coulomb Energy, b) Dispersion Energy, c) Total Energy. Lines thickness is proportional to the intensity of the interaction (threshold = -6 kJ/mol).

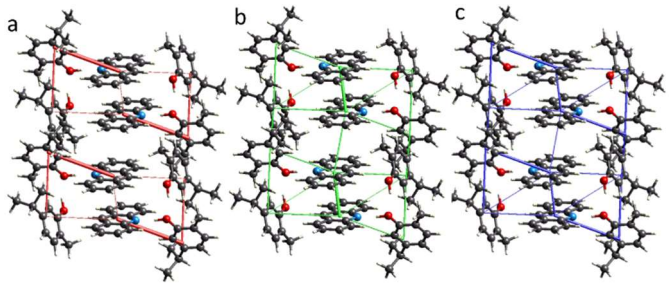

Figure 6. Energy framework Calculation performed on Acr:Car 1:2 at the B3LYP/6-31G(d,p) level of theory: a) Coulomb Energy, b) Dispersion Energy, c) Total Energy. Lines thickness is proportional to the intensity of the interaction (threshold = -6 kJ/mol).

as well as in binary cocrystals to assess whether a recurrent stabile geometry might be observed in cocrystals. The queries for the Conquest[61] interrogation were built asking for the P-P and A-A orientation (i.e. interplanar angle) between molecular dimers with closest atom-to-closest atoms distances not larger than 4.1 Å in binary cocrystals. Data were then analysed though CCDC Mercury 4.0 software package.[62]

This quite liberal distance threshold guarantees to have all possible reciprocal orientations between molecules in contact via π-π or CH-π interactions even though the number of records returned is clearly overestimated since also vicinal molecules not in contact with an effective interaction may also be included. In figure 7, we plotted the A-A and P-P interactions within the acridine or phenazine dimers, ranked according to the molecular offset (calculated from the centroids positions) against the molecular interplanar distance (fig. SI7). Only the effective interactions are here reported limiting the offset values to 7 Å (approximately corresponding to the size of the polycyclic molecules). The whole picture is reported in figures SI10 and SI11. Records were then coloured according to the angles registered between the molecular planes; the colour scale is reported rightmost in figure 7 ranging from blue (parallel molecular orientation) to red (orthogonal molecular orientation). The distributions of the interplanar angle within acridine or phenazine pairs observed in the analysed structures deposited in the CSD are respectively reported as polar histogram plots (insets in fig. 7). Acridine or phenazine molecules in cocrystals are generally oriented in a parallel fashion (interplanar angle < 10°), predominantly distributed in the range of interplanar distance compatible with the π-π interaction. Only very few exceptions report a different orientation (interplanar angle > 40°) generally related to larger

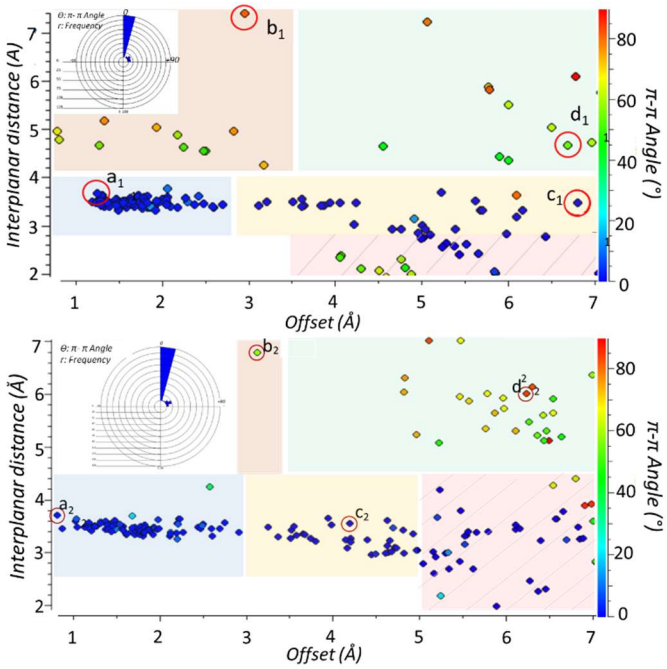

Figure 7. Faced acridine-acridine (A-A) (up) and phenazine-phenazine (P-P) (down) reciprocal orientation observed in analysed cocrystals. Molecular offset (Å) vs molecular interplanar distance (Å) scatter plot. Records are coloured according to the angles registered between the molecular planes ranging from blue (parallel molecular orientation) to red (orthogonal molecular orientation). a) Blue zone represents short interplanar distance and a modest coformers offset. b) Yellow zone represents large coformers offset with a modest interplanar distance. c) Orange zone represents modest coformers offset and a large interplanar distance. d) Green zone represents large coformers offset and an a noticeable interplanar distance. Inset: polar histogram reporting the distributions of the interplanar angle within acridine or phenazine pairs observed in the analysed structures.

molecular offset or larger interplanar distances. Records characterized by large offset and short interplanar distances are not considered in the statistical analysis since they represent side-by-side molecules not involved in any π-π or CH-π contact. Packing diagram representative of the A-A and P-P orientations are exemplified in figure 8. Surprisingly, P-P and A-A contact orientations distribution in pure phases is rather different with a remarkable bimodal distribution of the reciprocal orientation characterized by molecules paired either in parallel or T-shaped fashion (fig. SI12 and SI13). From the comparison of the acridine and phenazine distributions observed in the cocrystals with those observed in the coformer pure phases is evident that the two molecules adopt prevalently the parallel orientation when they are embedded within cocrystal structures. The analysis, thus, suggests that whenever phenazine or acridine are used as coformers in cocrystals, they do contribute to the overall packing energy by pairing themselves in a π-π stacking orientation.

In order to quantify this contribution in terms of energy stabilization, we have performed the packing energy calculation with CrystalExplorer[63] for Acr:Thy and Acr:Car and their phenazine analogous[17] at the B3LYP/6-31G(d,p) level of theory. In order to widen the case study, the same calculations have been carried out also for cocrystals with vanillin (Van) and

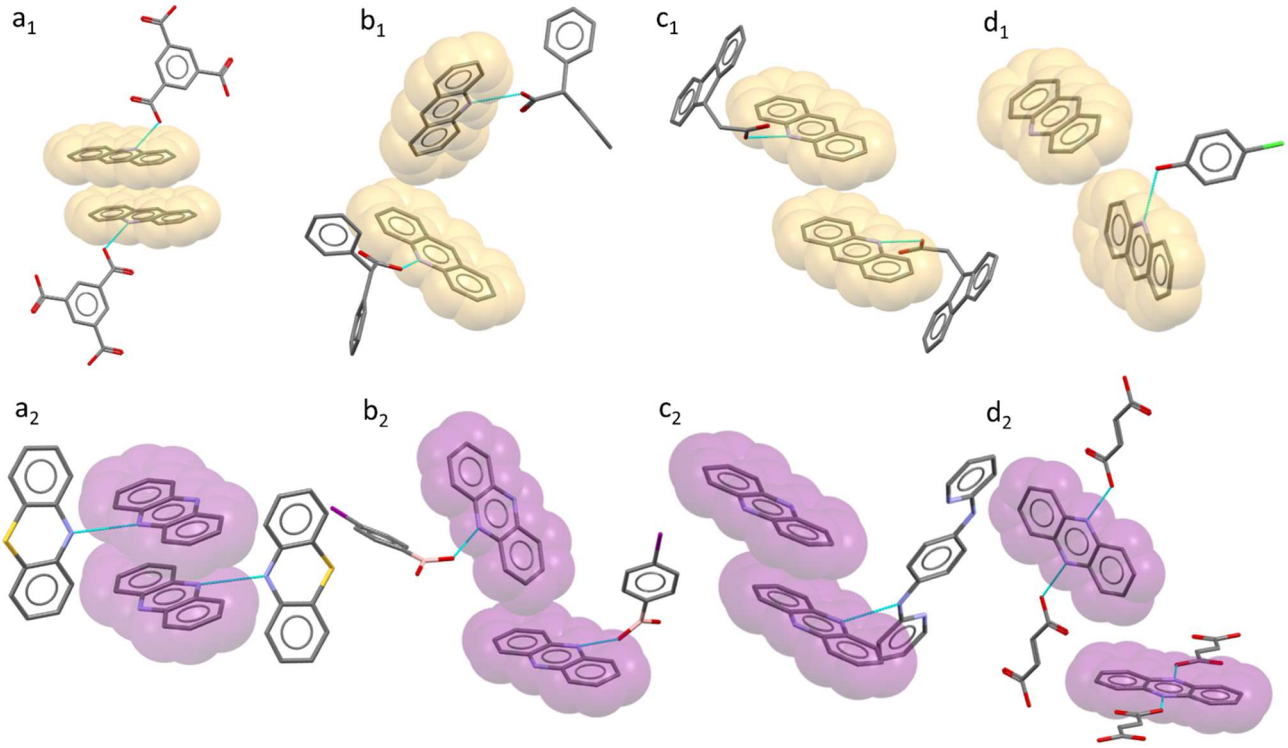

Figure 8. Exemplificative records of molecular orientations observed in acridine (a_1-d_1) and phenazine (a_2-d_2) based cocrystals, labelled in agreement to the scatter plots reported in figure 7. Acridine (yellow) and phenazine (purple) are emphasized in spacefil style. Hydrogen atoms are omitted for the sake of clarity. Dotted cyan lines represent H-bond between molecular partners.

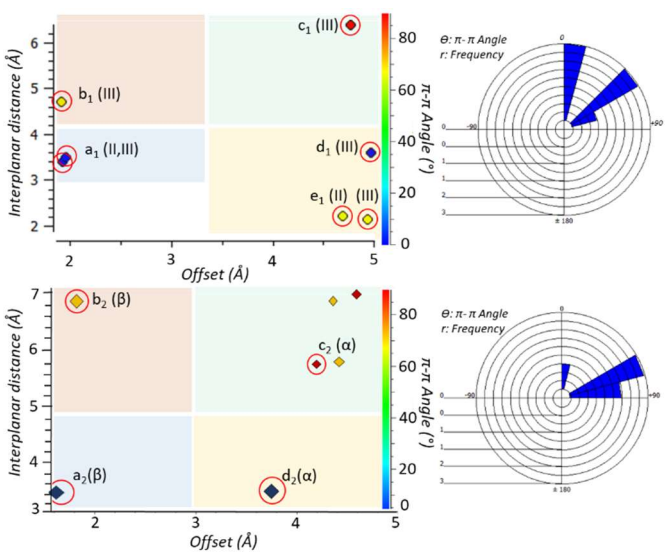

Figure 9. Molecular offset (Å) vs molecular interplanar distance (Å) scatter plots. Up. Acridine-acridine (A-A) reciprocal orientation observed in acridine II (a_1, e_1) and III (a_1-e_1) polymorphs. Down. Phenazine-phenazine (P-P) reciprocal orientation observed in phenazine α (c_2, d_2) and β (a_2, b_2) polymorphs. Records are coloured according to the angles registered between the molecular planes ranging from blue (parallel molecular orientation) to red (orthogonal molecular orientation). a) Blue zone represents short interplanar distance and modest coformers offset. b) Orange zone represents modest coformers offset and a large interplanar distance. c) Green zone represents large coformers offset and noticeable interplanar distance. d) Yellow zone represents short interplanar distance and large coformers offset. Hydrogen atoms are omitted for the sake of clarity. Rightmost: polar histograms reporting the bimodal distributions of the interplanar angle within acridine or phenazine pairs observed in the pure phases.

4-nitrophenol (4NP) (scheme 1), already reported in the literature.[35,64] Table 2 summarizes the results of the packing energy calculations performed on the selected cocrystals described above, and on acridine and phenazine pure phases, namely phenazine α, β and acridine II, III [35,65–67]. Coformer polymorphs differ by 0.5 kJ mol^{-1} for phenazine and up to 3.4 kJ mol^{-1} for acridine.

Firstly, we observed that the difference between the packing energy calculated for cocrystals and for pure coformer phases largely oscillates between small destabilizing values <1kJ mol^{-1} for Phe:Thy α to remarkably high energy stabilization of about 10 kJ mol^{-1} for Acr:Van. This shows that the nature of the MI is surely important to drive cocrystallisation.

We noted here that this estimate is a clear approximation since the actual stabilization of liquid MI into cocrystals should take into account the free energy rather than plain packing energy.[68]

From table 2, it appears that acridine is, in general, a better coformer, allowing higher stabilization energy for the cocrystals due to the formation of strong hydrogen bond interactions (values extracted from the energy framework calculations: Phe:Thy -43.5 kJ mol^{-1} [17], Acr:Thy -46.0 kJ mol^{-1}, Phe:Car -44.4 kJ mol^{-1} [17], Acr:Car -55.1 kJ mol^{-1}).

To understand whether the self-assembly of A-A and P-P dimers in the cocrystals may constitute a partial driving force for co-crystallization, we have unbundled the homomeric from the heteromeric interaction contributions to the packing energy.[48]

We have taken into account that selected cocrystals do present different stoichiometry ratio thus, for a cocrystal with 1:*n* stoichiometry, heteromeric energy contribution, namely E_{Hetero}

Table 2. Packing energy calculated at the B3LYP/6-31G(d,p) level of theory for acridine and phenazine pure phases and for selected cocrystals. Homomeric (A-A/P-P and MI-MI) and Heteromeric (A-MI/P-MI) energy contributions to the overall lattice energy are reported in kJ mol^{-1}.

	Packing Energy	A-A / P-P E_{Homo}	MI-MI E_{Homo}	A-MI / P-MI E_{Hetero}	A-MI / P-MI E_{Hetero_nom}
Phenazine α	-93.1	-	-	-	
Phenazine β	-92.6	-	-	-	
Acridine II	-96.7	-	-	-	
Acridine III	-93.3	-	-	-	
Phe:Thy α 1:1	-184.1	-45.1	-32.4	-106.6	-53.3
Phe:Thy β 1:1	-186.9	-43.4	-36.4	-107.1	-53.5
Phe:Car 1:2	-295.5	-40.7	-50.2	-154.4	-38.6
Phe:Van 1:1	-207.3	-52.2	-63.5	-91.7	-45.8
Phe:4NP 1:2	-330.5	-44.7	-53.6	-178.6	-44.7
Acr:Thy 1:1	-202.9	-42.2	-31.9	-128.8	-64.4
Acr:Car 1:2	-302.2	-42.5	-62.6	-134.5	-33.6
Acr:Van 1:1	-226.8	-48.0	-55.9	-122.9	-61.5
Acr:4NP 1:1	-208.6	-57.1	-37.8	-113.7	-56.9

is estimated as (1). In order to compare the stabilization ascribed to each kind of interactions, E_{Hetero_norm} is computed as (2), taking into account that for each A-A or P-P self-interaction, two hetero A-MI / P-MI interactions are present for each MI unit.

(1) $E_{Hetero} = PE - E_{Homo}(AAorPP) - nE_{Homo}\ (MI\ MI)$

(2) $E_{Hetero\_norm} = \frac{E_{Hetero}}{2n}$

The packing energy calculations returned that phenazine and acridine self-interactions range between -40.7 kJ mol^{-1} and -57.1 kJ mol^{-1}, estimated in a percentage contribution of the total packing energy of 20.8–27.4%, in case of 1:1 stoichiometry, and 13.5–14.1% in case of 1:2 stoichiometry. In case of higher stoichiometry ratio, coformer homomeric interaction do contribute less to the total energy since they are diluted into the cocrystal structural environment. The molecule of interest homomeric interactions oscillate between -31.9 and -63.5 kJ mol^{-1}, corresponding to 15.7 and 30.6% of the total packing energy, sensibly depending on the nature of the MI. The coformer-MI heteromeric interactions vary between -91.7 and -128.8 kJ mol^{-1} (for the 1:1 stoichiometry ratio) and -154.4 and -178.6 kJ mol^{-1} (for the 1:2 stoichiometry ratio), being the highest percentage of the packing energy (from 44.2% to 63.5 %). As a result, we can conclude that, even though the coformer-MI heteromeric interaction is the most important energy contribution to the overall cocrystal packing energy, acridine and phenazine typically participate with a quite constant non-negligible homomeric contribution due to the π-π stacking supramolecular interactions.

Conclusions

The stabilization of a cocrystal is based on the overall sum of interactions in the packing, which should drive the molecular partners to cooperate in building a new architecture, different from the ones of the pure phases. We usually focus on the new links created by the encounter of the two molecular partners, namely the heteromeric interactions between the molecule of interest and the coformer, but the ensemble of stabilizing contacts in the new architecture may include strong coformer homomeric interactions. Here we combined the calculation of heteromeric and homomeric interactions with a thorough analysis of the self-assembly trends found in the CSD for two very popular coformers, acridine and phenazine, and found that very often the two coformers adopt preferential homomeric packing geometry within cocrystals structures, bringing a dowry of stabilizing energy ranging between 21 and 28 % (-40.7 – -57.1 kJ mol^{-1}) into the common house. In other words, the π-π stacking supramolecular self interactions built by acridine and phenazine typically participate in cocrystals with a constant non-negligible contribution to the packing energy.

Experimental

General

All reagents were purchased from Sigma Aldrich and used without further purification.

Synthesis of Acr:Thy 1:1. 121.3 mg acridine (0.677 mmol) were added to 101.7 mg thymol (0.677 mmol) in a ceramic mortar. The powder mixture was grinded for 10 minutes resulting in a white fine powder. X-Ray Powder Diffraction analysis performed on the product outcome revealed that the titled compound was obtained but some extra peaks were also detected in the pattern. The product was therefore purified dissolving it in 3 mL of diethylether in a semi-closed 5 mL vial and left to evaporate under the fume hood aspiration. After 7 days, colourless single crystals were obtained and subsequently used for crystallographic analysis.

Synthesis of Acr:Car 1:2. 114.0 mg acridine (0.636 mmol) were added to 0.098 ml carvacrol (0.636 mmol) in a ceramic mortar. The mixture thus obtained was ground with a pestle under fumehood aspiration for 10 minutes until a pale-yellow homogeneous mixture is obtained. X-Ray Powder Diffraction analysis performed on the product outcome revealed that the titled compound was obtained but some extra peaks were also detected in the pattern. The product was therefore purified dissolving it in 2.5 mL of diethylether. The as obtained clear solution was then transferred in a 5 mL vial and left overnight under the fume hood to let the solvent evaporate. Pale yellow prism single crystals were obtained and used for crystallographic analysis.

Thermal Analyses. Differential scanning calorimetry analysis of Acr:Thy and Acr:Car was performed with a PerkinElmer Diamond equipped with a model ULSP 90 ultracooler. Heating was carried out in closed 5 µL Al-pans at 5 °C/min in the temperature range -25 to 120 °C. The measurement was performed at atmospheric pressure under a constant nitrogen flow (20 µL min^{-1}) The enthalpy of the endothermic or exothermic events is determined by the integration of the area under the differential scanning calorimetry (DSC) peak, which is reported in J/g (see Supporting Information).

Single Crystal X-ray Diffraction. SC-XRD analysis was performed on single crystal samples at 200 K on a SMART APEX2

diffractometer using Mo Kα radiation (λ = 0.71073 Å) for Acr:Car 1:2; Lorentz polarization and absorption correction were applied. Data for Acr:Thy 1:1 were collected at 100 K under nitrogen flux at Elettra Synchrotron (Trieste, Italy) at the XRD1 beamline with X-ray synchrotron radiation source and a NdBFe Multipole Wiggler (Hybrid linear) insertion device. Beam energy was set at 4.27 keV with a power of 8.6 kW and a beamsize fwhm of 2.0 × 0.37 mm (0.7 × 0.2 mm fwhm beam size on the sample) with photon flux 10^{12}–10^{13} ph/sec. Pilatus 2 M detector was used to collect the data; synchrotron data were processed by using XDS software.[69] Structures were solved by direct methods using SHELXT[70] and refined by full-matrix least-squares on all F^2 using SHELXL[71] implemented in Olex2.[72] ORTEP diagrams are reported in Supporting Information. Crystallographic data for Acr:Car and Acr:Thy have been deposited with the Cambridge Crystallographic Data Centre as supplementary publication CCDC 1986371-1986372.

Powder X-ray Diffraction. PXRD analyses were performed to check the purity of the samples. PXRD data were collected on a Thermo Scientific ARL XTRA diffractometer in theta−theta Bragg−Brentano geometry with CuKα radiation. All experimental data were refined with a Pawley fit against the cell parameters extracted from SCXRD analyses optimized at room temperature.

Packing Energy Calculations (PEC). PEC were performed using CrystalExplorer17 software package (2017 University of Western Australia) at the B3LYP/6-31G(d,p) level of theory with a radius > 20 Å. To isolate the contribution due to the P-P or A-A homo-interactions to the overall packing energy (E_{HOMO}) in cocrystals, two different modified versions of the original cif file were derived, each individually reporting the coordinates of coformers the same kind. Packing energy were than calculated also over those modified structures.

Abbreviations

MI = Molecule of Interest, Phe = Phenazine, Acr = Acridine, P-P = Phenazine-Phenazine, A-A = Acridine-Acridine, Phe:Thy = Phenazine:Thymol 1:1 cocrystal, Phe:Car = Phenazine:Carvacrol 1:2 cocrystal, Phe:Van = Phenazine:Vanilline 1:1 cocrystal, Phe:4NP = Phenazine:4-NitroPhenol 1:2 cocrystal, Acr:Thy = Acridine:Thymol 1:1 cocrystal, Acr:Car = Acridine:Carvacrol 1:2 cocrystal, Acr:Van = Acridine:Vanilline 1:1 cocrystal, Acr:4NP = Acridine:4-Nitrophenol 1:1 cocrystal, PEC = Packing Energy Calculation

Conflicts of interest

There are no conflicts to declare

Acknowledgements

Dr Nicola Demitri at the XRD1 beamline of Elettra Synchrotron, (Trieste, Italy) is thanked for helpful assistance in data collection. This work was funded by the Ministero delle Politiche Agricole, Alimentari, Forestali (MIPAAF) by granting for the project PAC/Packaging Attivo Crystallino. This work has used resources available from the "Department of Excellence" Project of the Italian MIUR Ministry. COST Action CA18112 - Mechanochemistry for Sustainable Industry is also acknowledged. The Laboratorio di Strutturistica Mario Nardelli at the University of Parma is acknowledged for in-house data collection facilities.

Notes and references

1 A. D. Bond, *CrystEngComm*, 2007, **9**, 833–834.
2 J. Zukerman-Schpector and E. R. T. Tiekink, *Zeitschrift für Krist.*, 2008, **223**, 233–234.
3 S. Aitipamula, R. Banerjee, A. K. Bansal, K. Biradha, M. L. Cheney, A. R. Choudhury, G. R. Desiraju, A. G. Dikundwar, R. Dubey, N. Duggirala, P. P. Ghogale, S. Ghosh, P. K. Goswami, N. R. Goud, R. R. K. R. Jetti, P. Karpinski, P. Kaushik, D. Kumar, V. Kumar, B. Moulton, A. Mukherjee, G. Mukherjee, A. S. Myerson, V. Puri, A. Ramanan, T. Rajamannar, C. M. Reddy, N. Rodriguez-Hornedo, R. D. Rogers, T. N. G. Row, P. Sanphui, N. Shan, G. Shete, A. Singh, C. C. Sun, J. A. Swift, R. Thaimattam, T. S. Thakur, R. Kumar Thaper, S. P. Thomas, S. Tothadi, V. R. Vangala, N. Variankaval, P. Vishweshwar, D. R. Weyna and M. J. Zaworotko, *Cryst. Growth Des.*, 2012, **12**, 2147–2152.
4 C. B. Aakeröy and D. J. Salmon, *CrystEngComm*, 2005, **7**, 439–448.
5 P. A. Wood, N. Feeder, M. Furlow, P. T. A. Galek, C. R. Groom and E. Pidcock, *CrystEngComm*, 2014, **16**, 5839.
6 M. K. Corpinot and D. K. Bučar, *Cryst. Growth Des.*, 2019, **19**, 1426–1453.
7 D. Braga, F. Grepioni and L. Maini, *Chem. Commun.*, 2010, **46**, 6232.
8 G. R. Desiraju, *J. Am. Chem. Soc.*, 2013, 135, 9952–9967.
9 F. H. Allen, W. D. S. Motherwell, P. R. Raithby, G. P. Shields and R. Taylor, *New J. Chem.*, 1999, **23**, 25–34.
10 S. R. Fukte, M. P. Wagh and S. Rawat, *Int. J. Pharm. Pharm. Sci.*, 2014, **6**, 9–14.
11 L. Brammer, *Chem. Soc. Rev.*, 2004, 33, 476–489.
12 A. Bacchi and P. Pelagatti, *Chem. Commun.*, 2016, **52**, 1327–1337.
13 P. P. Mazzeo, A. Bacchi and P. Pelagatti, *Coord. Chem. Rev. Submitt.*
14 D. Balestri, P. Scilabra, C. Carraro, A. Delledonne, A. Bacchi, P. P. Mazzeo, L. Carlucci and P. Pelagatti, *CrystEngComm*, 2019, **21**, 6365–6373.
15 C. Aakeroy, *Acta Crystallogr. Sect. B Struct. Sci. Cryst. Eng. Mater.*, 2015, **71**, 387–391.
16 B. Sandhu, A. S. Sinha, J. Desper and C. B. Aakeroy, *ChemComm* , 2018, **54**, 4657–4660.
17 P. P. Mazzeo, C. Carraro, A. Monica, D. Capucci, P. Pelagatti, F. Bianchi, S. Agazzi, M. Careri, A. Raio, M. Carta, F. Menicucci, M. Belli, M. Michelozzi and A. Bacchi, *ACS Sustain. Chem. Eng.*, 2019, **7**, 17929–17940.
18 M. Karimi-Jafari, L. Padrela, G. M. Walker and D. M. Croker, *Cryst. Growth Des.*, 2018, 18, 6370–6387.
19 J. W. Steed, *Trends Pharmacol. Sci.*, 2013, **34**, 185–193.

20 N. Schultheiss, S. Bethune and Jan-Olav Henck, *CrystEngComm*, 2010, **12**, 2436–2442.
21 A. Bacchi, D. Capucci, M. Giannetto, M. Mattarozzi, P. Pelagatti, N. Rodriguez-Hornedo, K. Rubini and A. Sala, *Cryst. Growth Des.*, 2016, **16**, 6547–6555.
22 N. Jagadeesh Babu and A. Nangia, *Cryst. Growth Des*, 2011, **11**, 2662–2679.
23 J. Zhang ab and ne M. Shreeve, *CrystEngComm*, 2016, **18**, 6124–6133.
24 D. Capucci, D. Balestri, P. P. Mazzeo, P. Pelagatti, K. Rubini and A. Bacchi, *Cryst. Growth Des.*, 2017, **17**, 4958–4964.
25 G. R. Desiraju, *Angew. Chemie Int. Ed. English*, 1995, 34, 2311–2327.
26 I. Bassanetti, S. Bracco, A. Comotti, M. Negroni, C. Bezuidenhout, S. Canossa, P. P. Mazzeo, L. Marchiò and P. Sozzani, *J. Mater. Chem. A*, 2018, **6**, 14231.
27 H. Wahl, D. A. Haynes and T. le Roex, *South African J. Chem.*, 2016, **69**, 35–43.
28 M. K. Corpinot, S. A. Stratford, M. Arhangelskis, J. Anka-Lufford, I. Halasz, N. Judaš, W. Jones and D. K. Bučar, *CrystEngComm*, 2016, **18**, 5434–5439.
29 M. C. Etter, *Acc. Chem. Res.*, 1990, **23**, 120–126.
30 A. D. Buckingham, J. E. Del Bene and S. A. C. McDowell, *Chem. Phys. Lett.*, 2008, **463**, 1–10.
31 D. Balestri, P. P. Mazzeo, C. Carraro, N. Demitri, P. Pelagatti and A. Bacchi, *Angew. Chem. Int. Ed.*, 2019, **58**, 17342–17350.
32 G. Cavallo, P. Metrangolo, R. Milani, T. Pilati, A. Priimagi, G. Resnati and G. Terraneo, *Chem. Rev.*, 2016, 116, 2478–2601.
33 P. P. Mazzeo, C. Carraro, A. Arns, P. Pelagatti and A. Bacchi, *Cryst. Growth Des.*, 2020, **20**, 636–644.
34 D. Musumeci, C. A. Hunter, R. Prohens, S. Scuderi and J. F. McCabe, *Chem. Sci.*, 2011, **2**, 883.
35 D. Braga, F. Grepioni, L. Maini, P. P. Mazzeo and K. Rubini, *Thermochim. Acta*, 2010, **507**–**508**, 1–8.
36 E. Schur, E. Nauha, M. Lusi and J. Bernstein, *Chem. - A Eur. J.*, 2015, **21**, 1735–1742.
37 A. Lemmerer, D. A. Adsmond, C. Esterhuysen and J. Bernstein, *Cryst. Growth Des.*, 2013, **13**, 3935–3952.
38 M. Lusi, I. J. Vitorica-Yrezabal and M. J. Zaworotko, *Cryst. Growth Des.*, 2015, **15**, 4098–4103.
39 S. Skovsgaard and A. D. Bond, *CrystEngComm*, 2009, **11**, 444–453.
40 T. Lee, H. R. Chen, H. Y. Lin and H. L. Lee, *Cryst. Growth Des.*, 2012, **12**, 5897–5907.
41 C. R. Taylor and G. M. Day, *Cryst. Growth Des.*, 2018, **18**, 892–904.
42 B. Sarma, L. S. Reddy and A. Nangia, *Cryst. Growth Des.*, 2008, **8**, 4546–4552.
43 T. Grecu, H. Adams, C. A. Hunter, J. F. McCabe, A. Portell and R. Prohens, *Cryst. Growth Des.*, 2014, **14**, 1749–1755.
44 T. Grecu, C. A. Hunter, E. J. Gardiner and J. F. McCabe, *Cryst. Growth Des.*, 2014, **14**, 165–171.
45 A. Oliver, C. A. Hunter, R. Prohens and J. L. Rosselló, *J. Comput. Chem.*, 2018, **39**, 2371–2377.
46 J. McKenzie and C. A. Hunter, *Phys. Chem. Chem. Phys.*, 2018, **20**, 25324–25334.
47 C. A. Hunter, *Angew. Chem. Int. Ed.*, 2004, 43, 5310–5324.
48 A. Gavezzotti, V. Colombo and L. Lo Presti, *Cryst. Growth Des.*, 2016, **16**, 6095–6104.
49 A. Gavezzotti and L. Lo Presti, *Cryst. Growth Des.*, 2016, **16**, 2952–2962.
50 A. Gavezzotti and L. Lo Presti, *Cryst. Growth Des.*, 2015, **15**, 3792–3803.
51 J. G. P. Wicker, L. M. Crowley, O. Robshaw, E. J. Little, S. P. Stokes, R. I. Cooper and S. E. Lawrence, *CrystEngComm*, 2017, **19**, 5336–5340.
52 H. Barua, A. Gunnam, B. Yadav, A. Nangia and N. R. Shastri, *CrystEngComm*, 2019, **21**, 7233–7248.
53 L. Roca-Paixão, N. T. Correia and F. Affouard, *CrystEngComm*, 2019, **21**, 6991–7001.
54 M. A. Solomos, T. A. Watts and J. A. Swift, *Cryst. Growth Des.*, 2017, **17**, 5073–5079.
55 C. R. Groom, I. J. Bruno, M. P. Lightfoot and S. C. Ward, *Acta Crystallogr. Sect. B Struct. Sci. Cryst. Eng. Mater.*, 2016, **72**, 171–179.
56 A. C. V. Solano and C. R. de Gante, *Food Bioprocess Technol.*, 2012, **5**, 2522–2528.
57 S. Borrego, O. Valdés, I. Vivar, P. Lavin, P. Guiamet, P. Battistoni, S. Gómez de Saravia and P. Borges, *ISRN Microbiol.*, 2012, **2012**, 1–7.
58 A. Rivera, J. Sadat-Bernal, J. Ríos-Motta and M. Bolte, *Crystals*, 2019, **9**, 520.
59 A. J. Edwards, C. F. Mackenzie, P. R. Spackman, D. Jayatilaka and M. A. Spackman, *Faraday Discuss.*, 2017, **203**, 93–112.
60 C. F. Mackenzie, P. R. Spackman, D. Jayatilaka and M. A. Spackman, 2017, **4**, 575–587.
61 I. J. Bruno, J. C. Cole, P. R. Edgington, M. Kessler, C. F. Macrae, P. Mccabe, J. Pearson and R. Taylor, *Acta Cryst Sec. B*, 2002, **B58**, 389–397.
62 C. F. Macrae, I. Sovago, S. J. Cottrell, P. T. A. Galek, P. Mccabe, E. Pidcock, M. Platings, G. P. Shields, J. S. Stevens, M. Towler and P. A. Wood, *J. Appl. Cryst*, 2020, **53**, 226–235.
63 M. J. Turner, J. J. McKinnon, S. K. Wolff, D. Grimwood, D. J. Spackman, P. R. Jayatilaka and M. A. Spackman, 2017.
64 A. Nayak and V. R. Pedireddi, *Cryst. Growth Des.*, 2016, **16**, 5966–5975.
65 F. H. Herbstein and G. M. J. Schmidt, *Acta Cryst.*, 1955, **8**, 406.
66 W. Jankowski and M. Gdaniec, *Acta Cryst. Sec. C*, 2002, **C58**, o181–o182.
67 X. Mei and C. Wolf, *Cryst. Growth Des.*, 2004, **4**, 1099–1103.
68 A. J. Cruz-Cabeza, S. E. Wright and A. Bacchi, *CrystEngComm Submitt.*
69 W. Kabsch, *Acta Cryst. Sec. D*, 2010, **66**, 125–132.
70 G. M. Sheldrick, *Acta Cryst A*, 2015, **71**, 3–8.
71 G. M. Sheldrick, *Acta Cryst. Sec. C*, 2015, **71**, 3–8.
72 O. V. Dolomanov, L. J. Bourhis, R. J. Gildea, J. A. K. Howard and H. Puschmann, *J. Appl. Crystallogr.*, 2009, **42**, 339–341.